Spectroscopic Investigation of Photoinduced Charge Separation and Recombination in Solid Polymers

Guohong Zhang and J. Kerry Thomas*

Department of Chemistry and Biochemistry, University of Notre Dame, Notre Dame, Indiana 46556

Received: October 30, 1997; In Final Form: January 28, 1998

Charge generation in polymer films following photoexcitation of charge-transfer complexes and UV two-photon ionization of aromatic dopants was studied by transient absorption spectroscopy. Charge separation from photoinduced contact ion pairs is due to the hole migration away from the geminate radical anions during the lifetime of the exciplex, which occurs by a hopping mechanism. Hole trapping at dimeric sites and subsequent charge recombination give rise to delayed exterplex emission. In resonant two-photon photoionization experiments, radical cations of aromatic molecules and excess electrons were produced as the primary charged species. The thermalization length of electrons ejected from perylene by 337-nm photons was measured as 36 Å in solid polystyrene. Within the first 1 ns, reactions of electrons with polymer matrixes compete with the geminate electron−cation recombination, which leads to electron trapping and charge separation, with trapped ions stable up to milliseconds of time. Among the polymers studied, polystyrene shows the lowest reactivity and therefore the lowest yield of charge separation, $\psi_{PS} = 2.4\%$, whereas poly(vinylbenzyl chloride) scavenges nearly all the excess electrons and exhibits the highest charge separation yield, $\psi_{PVBC} = 1$ at 210 K. Subsequent recombination of charge carriers trapped at different depths in solid polymer matrixes is diffusion limited over a wide dynamic range. The ion neutralization kinetics gradually evolves from geminate in nature to a homogeneous second-order reaction. The diffusivities of charge carriers were measured as 7.5×10^{-10} cm^2/s for Cl^- in poly(vinylbenzyl chloride), 2.2×10^{-10} cm^2/s for $CO_2^{-\bullet}$ in poly(benzyl methacrylate), and 7.0×10^{-12} cm^2/s for $CO_2^{-\bullet}$ in poly(methyl methacrylate).

Introduction

An interesting feature of photochemistry in polymers, which determines the photoelectronic properties of an important class of materials called photoconductive polymers, is derived from charge-transfer (CT) reactions. Photogeneration of charge carriers in polymers has been studied with a potential application in developing polymer-based Xerographic materials.[1−3] The performance of photoconductive polymers is mechanistically elucidated in terms of two closely related processes; these are, photoinduced charge generation and transport of charge carriers. These processes have been empirically described by the classical Onsager theory in which parameters such as charge separation yield and mobilities of charge carriers are abstracted without detailed knowledge on the molecular level.[1,4,5] Recent advances in time-resolved spectroscopic techniques and electron transfer theory have revitalized the research concerning the microscopic mechanisms of photoconductivity in polymers.[6−9]

Generally, photoinduced charge separation in polymers can be achieved in three different ways: ionization from low-lying excited states of polymers or dopants, ionization from excited-state CT complexes, and ionization from high Rydberg states. The charge generation efficiency from excited states of polymer-bound chromophores [e.g., poly(vinylcarbazole), abbreviated as PVCz] and dopants (e.g., *N*-isopropylcarbazole dispersed in polycarbonate matrix) is as low as $\Phi \approx 10^{-5}$ at zero field strength. High electric fields are applied to enhance the quantum yield of ionization. Charge transport in solid polymer matrixes occurs by a hopping mechanism. The measured electric current is attributed to the repetitive electron transfer (ET) from neutral molecules to cation radicals for *p*-type conduction, and from anion radicals to neutral molecules for *n*-type conduction. As a result, a strong dependence of the hole drift mobility on the dopant or chromophore concentration is observed.[1]

Photoexcitation of polymers in the presence of electron acceptors also leads to charge generation.[5,9] The entire process by which mobile charge carriers are photogenerated via an ET reaction in any organic material involves several steps: initial production of local excited states by incoming photons, ET quenching of excited states and formation of contact ion pairs, geminate ion recombination, and production of free charge carriers. Charge recombination within geminate ion pairs, including exciplex formation, is always a competing process that limits the quantum yield of photogeneration, Φ. The efficiency of photogeneration is normally very low, and the quantum yields are typically $\sim 10^{-3}-10^{-2}$. The effect of applied electric fields on Φ has been well reproduced by the Onsager theory.[1,5] A large thermalization distance of $\sim$20 Å is usually deduced from the Onsager model for initially produced contact ion pairs in most organic materials.[1,5,10] However, the expected excess energy dependence of the so-called "thermalization distance" has not been experimentally observed.[11] The early stage of the CT processes starting with the contact ion pair and then changing to a more loosely bound ion pair is not considered in the Onsager model. A general model proposed by Noolandi[12] is used in this work to describe the early charge separation process.

Little work on photoionization of dopant molecules from high Rydberg states has been reported in polymer systems, although ionization of molecules by dumping photon energy up to 7−10 eV in the liquid phase has been well documented.[13,14] Different distribution functions were used to describe the initial position of the thermalized electron around the parent cation. Diffusion-controlled geminate kinetics leads to neutralization of the primary charge carriers and to the formation of free ions.[15] Both pulse radiolysis[16] and laser photolysis[13,14] have shown that the recombination of geminate electron−cation pairs in nonpolar liquids occurs on the picosecond time scale and is attributed to

S1089-5639(98)00030-9 CCC: $15.00
Published on Web 03/26/1998

the high mobility of the excess electrons under the influence of the Columbic interaction between the geminate electron and cation. The diffusivity of the shallowly trapped electrons in hydrocarbon liquids is normally on the order of 10^{-3} cm^2/s. However, processes in polymers induced by radiation with energy between the high and the low limits are not well understood. Many questions remain unanswered about charge generation, trapping, and transport in polymers: Can we photoionize solute molecules in polymer matrixes just as in liquid solutions? What is the initial charge separation? Are polymer matrixes capable of trapping excess electrons? Could rigid polymers help separate and stabilize the charged species? The effects of solid polymers on ionization and subsequent charge separation are examined in this work.

The nature of transport of electronic charges through solid polymers is another issue to be addressed. In contrast to the diffusive transport of charge carriers in molecular liquids, where diffusion (D) is on the order of 10^{-5} cm^2/s, polymer matrixes impose a rigid restriction on the molecular transport. Therefore, in solid polymers, charge transport occurs via the following two possible processes: (1) a very slow diffusion of charge carriers through glassy matrixes; or (2) charge-hopping among the charge carrying components. The exact mechanism can be revealed from a spectroscopic study of recombination kinetics of specific charged species, which provides a different approach from the macroscopic photocurrent measurements.

Recent work in this laboratory has shown that high-energy radiation can induce efficient charge generation in nonpolar polymers, such as polystyrene (PS), in the absence of strong electron acceptors.[17] Solute cation radicals have been produced with a fairly large yield ($G \approx 1.6$ per 100 eV energy loss); and very fast positive hole transport ($\Lambda_h \approx 3 \times 10^{-5}$ cm^2/s) was proposed as being responsible for such an efficient charge generation. These results clearly indicate that the mechanism of charge separation in polymeric materials depends on the mode of excitation. It was also the purpose of this work to examine the effect of medium-energy radiation ($h\nu \sim 10$ eV) on solid polymers, which helps to bridge the gap between low-energy photochemistry and high-energy radiation chemistry in polymers. As part of our comparative studies between low-energy photochemistry and high-energy radiation chemistry of polymers, charge generation from CT excitation and UV two-photon ionization in solid polymers was investigated in this work. Laser photolysis techniques and fast kinetic spectroscopy were used to produce and monitor the ionic species in polymers. Charge separation and transport mechanisms were elucidated and compared with the results of high-energy radiolysis studies.

Experimental Section

Chemicals and Sample Preparation. Pyrene, perylene (Pe), *N*,*N*,*N*′,*N*′-tetramethylbenzidine (TMB), and 1,6-diphenylhexatriene (DPH) were obtained from Aldrich Chemical and used as ionization probes. Pyrene and TMB were purified by multiple recrystalliztion. 2,4,6-Trimethylbenzyl chloride (TMBC) and biphenyl from Aldrich were used as electron-trapping dopants in polystyrene. 1,2,4,5-Tetracyanobenzene (TCNB) also from Aldrich, was purified by multiple recrystallization from ethanol solution. Polymers used in this work include polystyrene (PS, MW, ~280 000), poly(styrene-*co*-acrilonitrile) with 75% styrene content (PSACN), polyacrylonitrile (PACN), poly(vinylbenzyl chloride) (PVBC, MW, ~55 000), poly(benzyl methacrylate) (PBM), poly(methyl methacrylate) (PMMA, MW, ~25 000), polyacrylonitrile (PACN), and polycarbonate (PC) were from Aldrich Chemical. Poly(2-phenyl ethyl methacrylate) (PPEM, MW, ~190 000) in a 25% toluene solution was obtained from Scientific Polymer Products, Inc. Films of PS, PVBC, PBM, PPEM, and PMMA with thicknesses of ~200 μm were cast from their benzene solutions with specific amounts of dopants. The PC films were cast from a 1,2-dichloroethane (DCE) solution of the polymer with added perylene. The concentration of perylene in the polymer films was controlled ~5 or ~10 mM. Film samples were covered by watch glasses and dried first in air for a day and then under reduced pressure for 8 h. The samples were further dried in air for 2 days before use. The TMBC-doped polystyrene films were only dried under watch glasses to avoid the possible loss of TMBC by extensive drying.

Instrumentation. A Varian Cary 3 UV−vis spectrophotometer was used to check the perylene absorbance at 337 nm in the film samples for charge generation yield measurements. An SLM spectrofluorometer (SFP-500C) was used to measure fluorescence emission and excitation spectra of polymer samples. Fluorescence lifetime measurements were made with an LN-100 Nitromite 337 nm laser (pulse width, ~0.3 ns; output, ~120 μJ/pulse) as the excitation source and a Hamamatsu microchannel plate PMT (R1644U) as the detector. Signals were captured by a computer-interfaced Tektronix 7912AD programmable digitizer. The time response of the entire measurement system was ~0.5 ns.

In transient absorption experiments, the following pulsed lasers were used to excite TCNB-PS CT complex and aromatic probe molecules in polymer films: (1) a Laser Photonics nitrogen gas laser (UV-24) with output at 337 nm (~5 mJ/pulse, ~10 ns duration); (2) a Lambda-Physik XeCl excimer laser (EMG-100) with output at 308 nm (~50 mJ, ~10 ns); (3) a mode-locked Nd:YAG laser with output at 355 nm (~5 mJ, ~35 ps). Laser photolysis was carried out under reduced pressure with polymer samples held in 2-mm quartz cells that were pumped to reduce the internal pressure down to 10^{-3} Torr for 15 min. The formation of TCNB anion radicals or perylene cation radicals was monitored by conventional transient absorption spectroscopy. Transient absorption spectra were collected by averaging 4−8 shots at each wavelength. Kinetic measurements were taken over a wide dynamic range, from 10^{-7} to 10 s. Transient signals within 10 ms were digitized by a computer-interfaced Tektronix 7912AD programmable digitizer, whereas signals on longer time scales were captured by a Tektronix TDS210 digital oscilloscope, and data acquisition was carried out using the Tektronix Wavestar software.

Theory and Simulation. For a quantitative understanding of the charge separation and recombination processes, the experimental measurements were simulated by available models for different mechanisms: (1) diffusion-controlled geminate ion recombination, as described by Noolandi and Hong;[12] (2) diffusion-influenced geminate recombination between slow moving charge carriers ($D < 10^{-8}$ cm^2/s); and (3) geminate recombination via long-range ET, as described by Tachiya and Mozumder.[18] Computer simulation of the first two processes involving molecular diffusion was performed by numerically solving the appropriate diffusion equations by a forward difference method.[19] The space grid and the time step were selected from a consideration of precision and stability.[20] A comparison between the simulated kinetics and the experimental observations over a wide dynamic range helps clarify the charge recombination mechanism in solid polymers.

Geminate Ion Recombination via Diffusion. The initial photoionization produces geminate electron−cation pairs that are well isolated from each other. We neglect the interaction among the ion pairs and treat them as isolated single pairs in a

statistical ensemble. This single-pair model has been used successfully in radiation chemistry.[15] For a single geminate ion pair in which the charge carriers with opposite charges diffuse in a dielectric media under the influence of mutual Columbic interaction, the movement of geminate ions can be adequately described by the Debye−Smoluchowski equation.[12] In a spherically symmetric system, the equation is written as follows.

$$\frac{\partial \rho}{\partial t} = D\left\{\frac{\partial^2 \rho}{\partial^2 r} + \left(\frac{2}{r} + \frac{R_c}{r^2}\right)\frac{\partial \rho}{\partial r}\right\} \quad (1)$$

The distribution function $\rho(r,t)$ is the probability density to find the geminate ions separated by distance r at time t. In eq 1, D is the mutual diffusion constant of geminate ions, and R_c is the Onsager radius $R_c = e^2/4\pi\epsilon_0\epsilon k_B T$. The pair survival probability at time t is $P(t)$:

$$P(t) = \int_0^\infty \rho(r,t)\, 4\pi r^2\, dr \quad (2)$$

The distribution function at $t = 0$ is defined in the initial condition:

$$\rho(r,0) = f(r) \quad (3)$$

For an ionization-induced electron−cation geminate pair, different forms of $f(r)$ have been used in the early work of radiation chemistry, including the exponential and the Gaussian functions. In the present work, a Gaussian function is used to describe the distribution of thermalized electrons:

$$f(r) = f_G(r) \propto \exp\left(-\frac{r^2}{b_G^2}\right) \quad (4)$$

where b_G is the distribution parameter that determines the most probable position of a thermalized electron around its parent cation.

Reaction between geminate ions at encounter is specified in the boundary condition at the reaction radius. For a diffusion-controlled charge recombination, the probability of reaction at encounter is assumed to be unity; that is,

$$\rho(r,t) = 0 \text{ for } r \le R_r \quad (5)$$

where R_r is the reactive radius for the recombination reaction.

The boundary condition at infinity is obvious:

$$\rho(r,t) = 0 \text{ for } r \rightarrow \infty \quad (6)$$

In the presence of charge scavengers, the scavenging reaction term was added to eq 1:

$$\frac{\partial \rho}{\partial t} = D\left\{\frac{\partial^2 \rho}{\partial^2 r} + \left(\frac{2}{r} + \frac{r_c}{r^2}\right)\frac{\partial \rho}{\partial r}\right\} - k_S C_S \rho \quad (7)$$

where C_S is the concentration of the scavenger. The bimolecular rate constant k_S for a diffusion-controlled scavenging reaction is given by the Smoluchowski relation:

$$k_S = 4\pi N_a R_S D \quad (8)$$

where R_S is the scavenging radius (cm), D is the mutual diffusion constant (cm^2/s), and N_a is the reduced Avogadro number (6.02×10^{20}).

Charge scavenging yield at different concentration was expressed by the following equation:

$$Y_S = \int_0^\infty dt \int_0^\infty dr\, 4\pi r^2 \left\{-\left(\frac{\partial \rho}{\partial t}\right)_S\right\} = \int_0^\infty dt\, k_S C_S P(t) \quad (9)$$

Using the relationship between the survival probability functions with and without a scavenger; that is,

$$P(t) = P_0(t) \exp\{-k_S C_S t\} \quad (10)$$

equation 9 can be rewritten as follows:

$$Y_S = C_S \int_0^\infty dt\, k(t)\, P_0(t) \exp\{-k_S C_S t\} \quad (11)$$

where $P(t)$ is the survival probability function at scavenger concentration C_S, and $P_0(t)$ is the survival probability function without any scavenger.

It is obvious from eq 1 that $\rho(r,Dt)$ and thus $P(Dt)$ are independent of D. The decay pattern does not depend on how fast charge carriers move, whether in liquid solutions or in solid polymers, but is only a function of the initial charge separation $f_G(r)$ and the Onsager length R_c. The decay function $P(t)$ for different D is a group of identical curves shifted from each other in parallel along the log t axis in a semilog plot $P(t)$ versus log t. As a result, the same decay curve as observed in liquid solutions on the picosecond time scale might be observed in solid polymers on a much longer time scale. Another feature of the diffusion-controlled geminate ion recombination is that the decay function $P(t)$ is not sensitive to the reactive radius. The effects of b_G and R_c on the decay function $P(Dt)$ are shown in Figure 1. Decay functions with a similar inverted "S" shape were also calculated by Noolandi by using a delta function $\delta(x = r_0)$ to describe the spatial distribution of thermalized electrons.[12]

Because the recombination within a geminate $e^- \cdots Pe^{+\bullet}$ pair produced in PS via photoionization is limited by the mobility of the excess electron, the model just described is used later to quantitatively understand the charge scavenging process in the polymer.

Diffusion-Influenced Geminate Ion Recombination. In this case, the ET interaction between two slow-moving ion radicals beyond their contact radius also leads to charge neutralization. Instead of implementing the recombination reaction at the contact radius, the ET reaction is included in eq 1 as a depletion term:

$$\frac{\partial \rho}{\partial t} = D\left\{\frac{\partial^2 \rho}{\partial^2 r} + \left(\frac{2}{r} + \frac{R_c}{r^2}\right)\frac{\partial \rho}{\partial r}\right\} - k(r)\rho \quad (12)$$

The ET rate $k(r)$ is defined conventionally:

$$k(r) = k_0 \exp\left(\frac{r - r_0}{a}\right) \quad (13)$$

where k_0 is the ET rate at encounter radius r_0, and a is the attenuation length.

The initial condition and the boundary condition at infinity are defined by eqs 3 and 6, respectively. However, a reflecting boundary condition is applied at $r = r_0$:

$$\left(\frac{\partial \rho}{\partial r}\right)_{r = r_0} = 0 \quad (14)$$

The decay function of the ion pair is given by eq 2. Figure 1c illustrates several decay curves $P(t)$ calculated using different D values. When D is large, the decay function is identical to the one derived from the diffusion-controlled geminate ion recombination. As D gets smaller and smaller, the decay

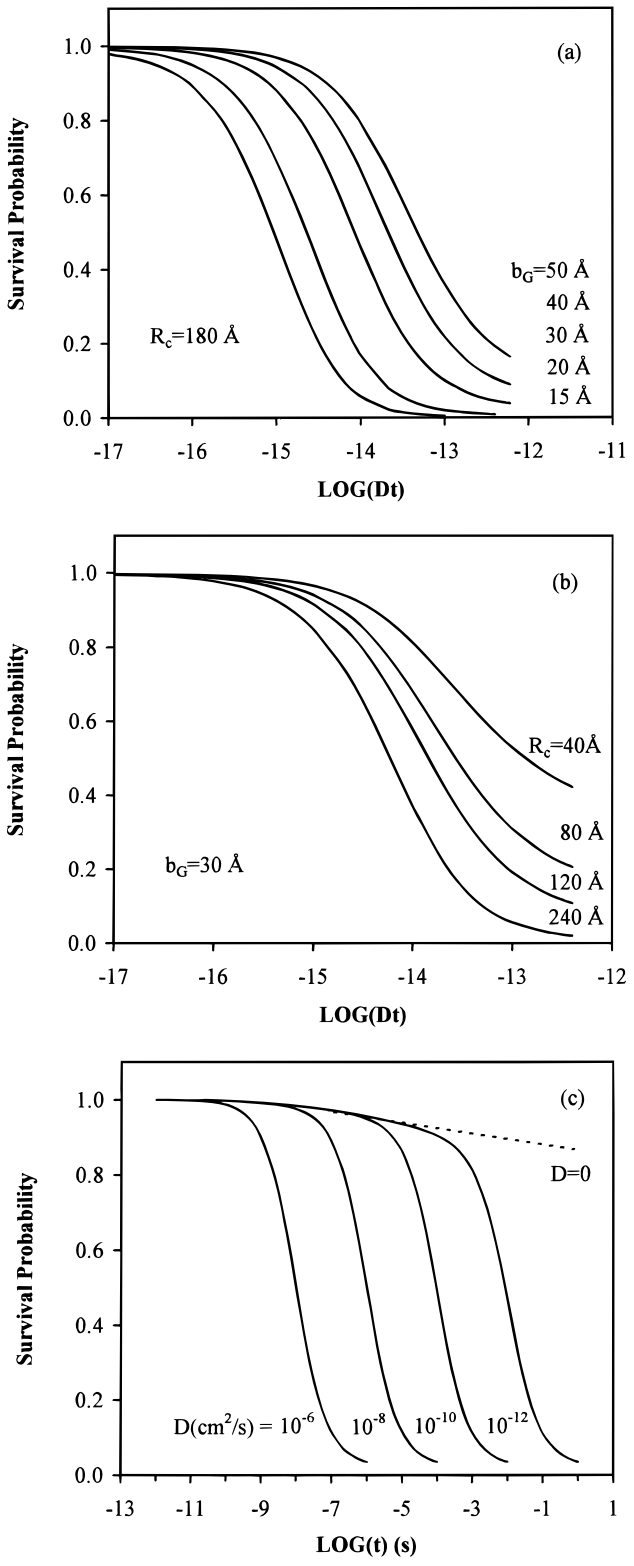

Figure 1. Computer simulation of diffusion-controlled geminate ion recombination kinetics. (a) Effect of the dispersion width; b_G = 15, 20, 30, 40, and 50 Å, R_c is fixed at 180 Å. (b) Effect of the Onsager length; R_c = 40, 80, 120, and 240 Å, b_G is fixed at 30 Å. (c) Effect of long-range electron transfer on geminate ion recombination; $\nu = 10^{10}$ s^{-1}, a = 0.8 Å, r_0 = 5 Å, b_G = 32 Å, R_c = 180 Å. Curves are calculated for different diffusion constants $D = 10^{-6}$, 10^{-8}, 10^{-10}, and 10^{-12} cm^2/s. The dashed line indicates the static limit (i.e., $D \rightarrow 0$; see text for definition of parameters).

functions gradually deviate from the diffusion-controlled pattern and show an early depletion due to the long-range ET reaction.

Geminate Ion Recombination via Electron Tunneling. When charge carriers are trapped in a rigid environment, the mobilities of the charge carriers are negligibly small ($D \rightarrow 0$), and geminate ion pairs recombine only via long-distance ET reaction. With $D = 0$ in eq 12, the decay function of geminate ion pairs is given by Tachiya[18] as:

$$P(t) = \int_0^\infty \exp\{-k(r)t\} f_G(r)\, 4\pi r^2\, dr \qquad (15)$$

It has been shown that a linear relationship exists between ln $P(t)$ and ln (νt) over a broad range of time scales. Such a flat decay kinetics over b_G/a (normally ~20−30 orders of magnitude in time) is characteristic of the geminate ion recombination via electron tunneling:

$$P(t) \propto (k_0 t)^{-a/b_G} \qquad (16)$$

The dash curve in Figure 1c shows the electron tunneling limit when $D \rightarrow 0$. It can be seen that recombination between slow-moving ion radicals in polymer matrixes is between the two limiting cases: the diffusion-controlled geminate ion recombination and the geminate ion recombination via electron tunneling. Variation of D mainly leads to shifting of decay function along the time axis with a slight depletion in the early part of the decay.

Results and Discussion

1. Charge Separation from Charge-Transfer Excitation. TCNB doped in PS readily forms the same ground-state CT complex with the phenyl groups as in liquid benzene derivatives. Figure 2a shows the absorption spectrum of a TCNB/PS film with [TCNB] = 20 mM. The additional shoulder appearing around 320 nm on the red side of the S_0-S_1 absorption band of PS is attributed to the CT complex between TCNB and PS. Excitation into this spectral region leads to a fluorescence spectrum shown in Figure 2a. The fluorescence is a combination of two bands, one centered at 400 nm and another shoulder around 500 nm. The former is due to the CT fluorescence from the $^1(TCNB^{-\bullet}\ PS^{+\bullet})^*$ exciplex, and the latter is attributed to the $^1(TCNB^{-\bullet}\ PS_2^{+\bullet})^*$ exterplex. Fluorescence from excitation of a TCNB−toluene CT complex exhibits a similar spectrum to the exterplex, also shown in Figure 2a. Picosecond experiments have shown that the complexation between the toluene cation radical and a ground-state toluene molecule occurs within 20 ps in liquid toluene right after the production of the $^1(TCNB^{-\bullet}Toluene^{+\bullet})^*$ exciplex,[21] which leads to the formation of a toluene dimer cation and a transformation of an exciplex to an exterplex. Such a fast dimer cation formation through rotational motion in glassy polymer is unlikely due to the restricted chain motion. As a result, fluorescence from the exciplex is mainly observed in PS. However, the appearance of the exterplex fluorescence is indicative of dimer cation formation via some other mechanism. Similar exterplex emission has also been found in PVCz and its model compounds.[22]

The time-resolved fluorescence measurements show that the exciplex decay is fairly exponential with a lifetime of 12.9 ns, indicating that the fluorescence is from a single configuration (i.e., contact ion pairs). The exterplex exhibits a very nonexponential decay with a long tail extending into microsecond region (Figure 2b). The slow component of the exterplex emission comes from geminate recombination between matrix-separated $TCNB^{-\bullet}$ and $PS_2^{+\bullet}$ ion pairs. This result was confirmed by nanosecond transient absorption measurements on TCNB/PS films after laser excitation at 337 nm. Figure 3a

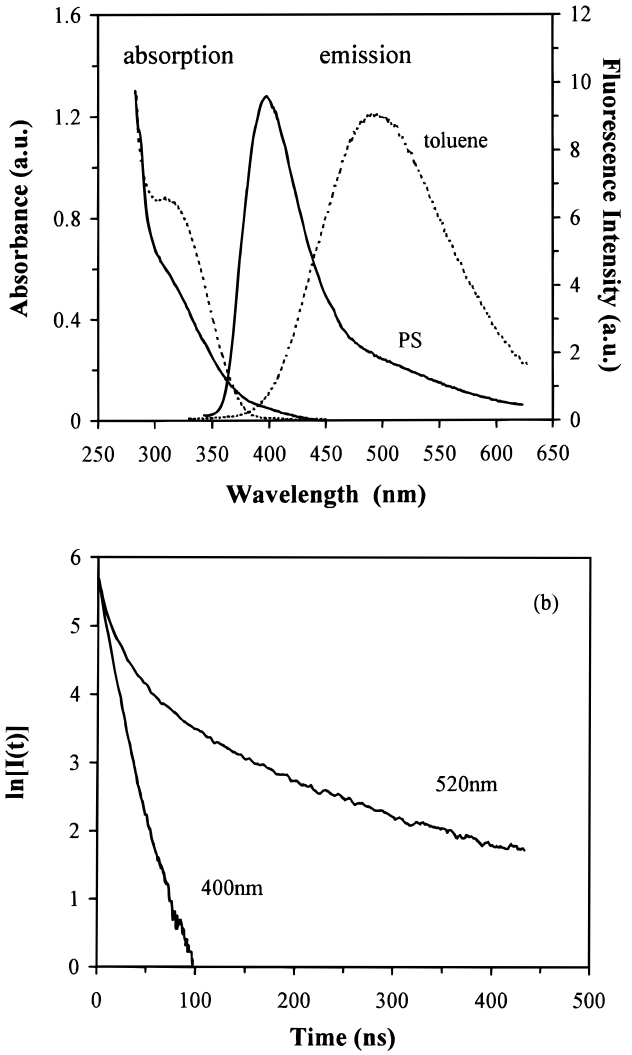

Figure 2. (a) Charge-transfer absorption and fluorescence emission spectra of a 2 mM TCNB−toluene solution (dashed lines) and 20 mM TCNB/PS film (solid lines). (b) Fluorescence decay traces of a TCNB/PS film monitored at 400 and 520 nm ($\lambda_{ex} = 337$ nm).

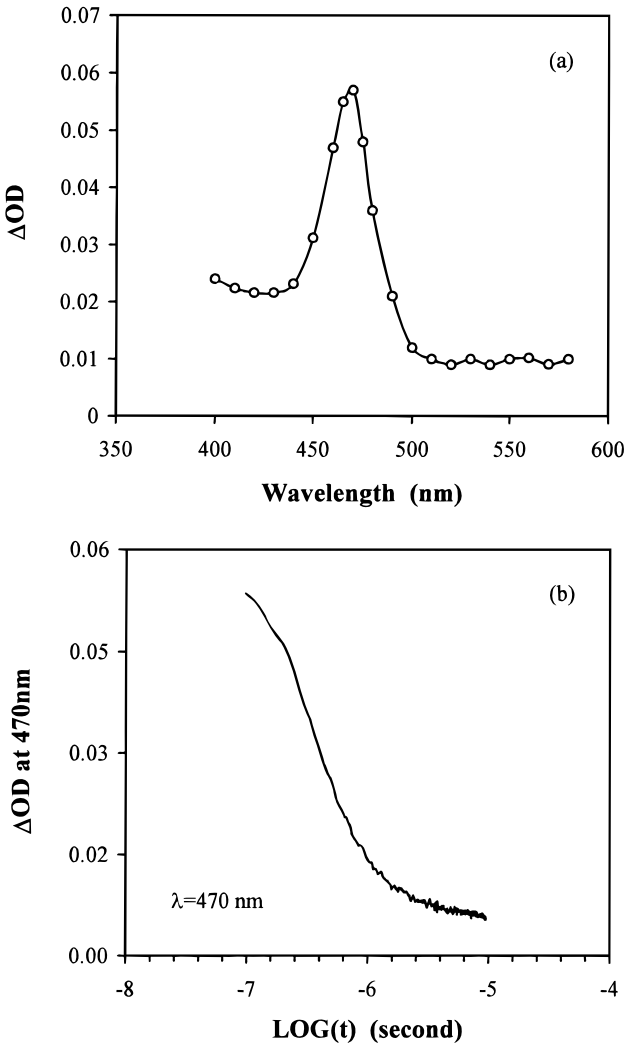

Figure 3. (a) Transient absorption spectrum of a 20 mM TCNB/PS film taken at 100 ns after the 337 nm laser pulse. (b) A semilog plot of the $TCNB^{-\bullet}$ decay kinetics in the PS film monitored at 470 nm.

SCHEME 1: Photoinduced Charge Transfer and Subsequent Charge Separation and Recombination Processes in TCNB-Doped Polystyrene

$$^1(PS^{+\cdot}TCNB^{-\cdot}) \xrightarrow{h\nu} {}^1(PS^{+\cdot}TCNB^{-\cdot})^{\bullet} \longleftrightarrow PS^{+\cdot} + TCNB^{-\cdot} \xrightarrow{trap} PS_2^{+\cdot} + TCNB^{-\cdot}$$

CT complex — contact ion pair — loose ion pair — matrix separated

↓ exciplex fluorescence, back electron transfer

↓ delayed exciplex fluorescence

shows the transient absorption specrtum of a 20 mM TCNB/PS film taken at 100 ns after the decay of exciplex. The single absorption band at 470 nm is attributed to the TCNB anion radical, $TCNB^{-\bullet}$.[23] The quantum yield of $TCNB^{-\bullet}$ measured at $t = 100$ ns is estimated to be $\Phi = 0.20$. This measurement utilizes the benzophenone triplet-excited state as a secondary standard (i.e., $\Phi_T = 1.0$).[24] Triplet benzophenone ($^3BP^*$) is produced in a 30 mM BP/PS film of the same thickness under the same excitation conditions as for the TCNB/PS film. The extinction coefficients of $^3BP^*$ and $TCNB^{-\bullet}$ are 7200 and 10 000 $M^{-1}cm^{-1}$, respectively.[23,24] The decay of $TCNB^{-\bullet}$ is nonexponential and gives rise to the exterplex emission on the microsecond time scale, which is much longer than the lifetime of the exterplex (estimated to be no larger than 41.8 ns from the TCNB−toluene data). Such a delayed fluorescence from ion recombination was also observed in TCNB-doped PVCz films.[22]

The charge separation and recombination processes just described are summarized in a coupled reaction scheme (Scheme 1), which is identical to that originally proposed by Noolandi.[12] Excitation of the CT complex first produces a Franck−Condon excited state that relaxes within 10 ps to form an exciplex that consists of a contact ion pair. Because the back ET reaction lies in the Marcus inverted region,[25] the slow ET rate within the contact ion pair results in a long lifetime of the exciplex ($\tau = 12.9$ ns). Such a long lifetime allows the hole on the phenyl group to migrate via a hopping mechanism a certain distance away from the geminate $TCNB^{-\bullet}$. Hole migration among the phenyl chromophores has been established as an important energy transfer pathway in our early work on high-energy radiolysis of polystyrene.[17] Recent picosecond laser photolysis studies of TCNB-doped PVCz films have also suggested that the loss of the original polarization of photoinduced ion pairs[8] and the positive CT from PVCz to *N*,*N*,*N*′,*N*′-tetramethyl-*p*-phenylenediamine (TMPD) is due to the hole migration.[9] The latter, in particular, provides a direct measurement of the distance (∼20 Å) that the hole on PVCz has to travel before being scavenged by TMPD.[9]

In contrast to the formation of the solvent-separated ion pair via molecular diffusion in liquids, hole migration under the influence of the strong Columbic interaction within the ion pair

($TCNB^{-\bullet}\cdots PS^{+\bullet}$) leads to a dynamic charge separation and recombination process. This migration transforms a contact ion pair described by a delta function $\delta(x = 0)$ into a matrix-separated ion pair with a wide spatial distribution. Without any depleting reaction, the distribution approaches a Boltzmann function at the long time limit.[12] However, the decay of the exciplex and the hole trapping by preexisting dimeric sites put a limit on the extent of charge separation. As a result, ~20% of the original contact ion pairs eventually escape the primary recombination and exist as matrix-separated ion pairs ($TCNB^{-\bullet}\cdots PS_2^{+\bullet}$). Subsequent hole-migration-controlled charge recombination on the microsecond time scale gives rise to the delayed exterplex fluorescence. The decay of $TCNB^{-\bullet}$ shown in Figure 3b corresponds to the exterplex emission at different times, as given in Figure 2b. Similar delayed fluorescence has also been observed in doped PVCz films and attributed to the charge recombination within the geminate pairs of the dimeric radical cation of PVCz and dopant radical anions.[22d]

Examination of the long-time behavior of the $TCNB^{-\bullet}$ decay kinetics indicated that it does not obey the square root law derived for the geminate ion recombination in homogeneous media,[12] presumably because of the dispersive nature of hole transport in solid polystyrene (i.e., the hole mobility is time dependent).[1a,3] Results of previous photoconductivity studies of PVCz indicated that the effective hole mobility is $\sim 10^{-7}$ cm^2/Vs at zero field when measurements were made on a time scale of 10 ms.[1a] This value corresponds to a migration constant of $10^{-8}-10^{-9}$ cm^2/s, indicating that the hole movement via charge hopping is much faster than the molecular diffusion in the polymer matrix ($D \approx 10^{-13}$ cm^2/s). However, an even faster rate of charge transport was observed at shorter times down to microseconds and nanoseconds.[26] This type of dispersive transport results from electronic hopping among localized states with significant fluctuation of site energies and has been established for singlet excitation migration in PS[27] and hole conductivity in PVCz.[9,26] Further photoconductivity data are needed to fully understand the hole transport in PS. It is pertinent to comment on the change of the transport properties with the molecular transformation of charge carriers from monomeric cations to dimeric cations via the intrinsic hole trapping. Our pulse radiolysis studies of PS show that the migration constant of the hole in form of monomeric cations $PS^{+\bullet}$ is $\sim 10^{-5}$ cm^2/s,[17] which is equivalent to a mobility (μ) of $\sim 10^{-3}$ cm^2/Vs. Similarly, the hole mobility in trap-free PVCz is $\sim 10^{-3}$ cm^2/Vs, with an activation energy E_a of ~0.1 eV.[28] After trapping at the dimeric sites, the hole exhibits a much lower mobility and a significantly higher activation energy of transport due to the stabilization by an additional binding energy of 0.3−0.4 eV; for example, $\mu \approx 10^{-7}$ cm^2/Vs and $E_a \approx 0.6$ eV in PVCz.[26,29,30]

2. Charge Separation from Two-Photon Ionization. Two-Photon Ionization in Polymers. In our experiments, aromatic molecules such as pyrene, TMB, DPH, and perylene are readily ionized in solid polymers by absorption of two UV photons, at any of three different wavelengths available (i.e., $\lambda_{ex} = 308$, 337, and 355 nm). For pyrene and TMB, transient absorption measurements of solute cation radicals suffer significant interference from the overlapping triplet absorption.[31] Meanwhile, a much lower ion yield was observed in photoionization of DPH in polymers. Among the solute molecules used, perylene was especially favored because of (1) its short-lived S_1 state and its low yield of triplet formation from intersystem crossing $\Phi_{isc} = 0.02-0.05$; (2) the well-separated perylene triplet and perylene cation radical absorption spectra; and (3) the strong absorption

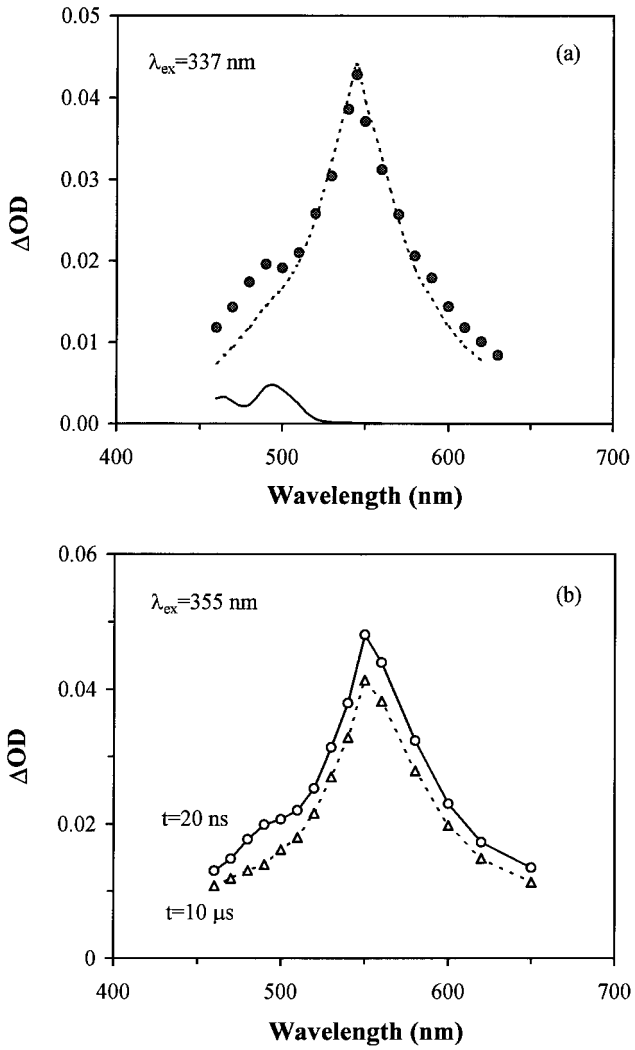

Figure 4. (a) Transient absorption spectrum of a 5 mM Pe/PBM film excited by 337 nm light (dots). Spectra of the perylene cation radical in an oxygenated 5 mM Pe/DCE solution (dashed line) and the triplet-excited state (solid line) in a 5 mM Pe−benzene solution sensitized by benzophenone are also shown for comparison. (b) Time-resolved absorption spectra of a 5 mM Pe/PSACN film excited by 355 nm light, taken in air at 20 ns (circles) and 10 μs (triangles) after the pulse.

of the perylene cation radical with $\epsilon = 49\,000$ M^{-1} cm^{-1} at 545 nm in liquid hydrocarbons.

Perylene was ionized in polymer films by a resonant two-photon process via the intermediate S_1 state, with absorbed energy that added up to 6.8, 6.5, and 6.3 eV for $\lambda_{ex} = 308$, 337, and 355 nm, respectively:

$$Pe \xrightarrow{h\nu} Pe^*(S_1) \xrightarrow{h\nu} Pe^{**}(S_n) \qquad (17a)$$

$$Pe^{**}(S_n) \xrightarrow{\text{autoionization}} Pe^{+\bullet} + e^- \xrightarrow{\text{trapping}} Pe^{+\bullet} + e^-_{tr} \qquad (17b)$$

primary recombination; secondary recombination

The second photon is absorbed by the S_1 state of perylene, which leads to electron ejection from the high Rydberg state (S_n) of perylene. Figure 4a illustrates the transient absorption spectrum of a 5-mM perylene-doped PBM film measured at 20 ns after the excitation by a 337-nm laser. Also shown in Figure 4a is the absorption spectrum of perylene cation radicals produced in an oxygenated (1 atm) DCE solution taken at 100 ns and the T_1-T_n absorption spectrum of perylene produced in 5 mM

perylene/benzene solution via benzophenone (20 mM) sensitization. The cation spectrum exhibits an absorption maximum at 545 nm, whereas the perylene triplet state has peaks at 495 and 465 nm with no absorption underneath the perylene cation radical spectrum >540 nm. Formation of the perylene cation was clearly seen in the polymer because the transient absorption in a laser-irradiated PBM film is simply a superposition of a strong cation spectrum and a weak triplet spectrum. A similar ionization process was observed in a 5-mM perylene-doped poly(acrylonitrile-*co*-styrene) film by excitation at 355 nm. The spectrum taken at 10 μs in air shows that oxygen removes the triplet, leaving the cation intact (Figure 4b).

Electron Trapping in Polymers. To compare the electron-trapping efficiencies in different polymers, quantum yields of charge separation were abstracted from the transient absorption measurements on the basis of a quantitative description of two-photon ionization processes (see *Appendix* for mathematical deriviation). The $Pe^{+\bullet}$ absorption signal A_{ion} is related to the charge separation yield ψ and the sample absorbance A_0 at the excitation wavelength through the following equation:

$$A_{ion} \propto \psi\left(\frac{1 - e^{-2A_0}}{2}\right) \tag{18}$$

The yield of charge separation in PVBC films was set to 1 and used as a standard because of complete scavenging of the excess electrons (i.e., $\psi_{PVBC} = 1$). The charge separation yields in other polymers were measured relative to PVBC. Two corrections were made in applying eq 18. First, it will be shown later in the section on the temperature effect on charge recombination that only 79% of initially produced perylene cations were measured on the nanosecond time scale at room temperature. This result is due to recombination of some of the geminate $Pe^{+\bullet}$ and Cl^- pairs separated by short distances. Complete charge separation on the microsecond time scale is observed at 210 K in PVBC. Hence, $\psi_{PVBC} = 0.79$ is used instead of $\psi_{PVBC} = 1$ at room temperature. Second, minor background absorption of the nitrogen laser (337 nm) by blank polymers such as PVBC and PACN was corrected using the following equation:

$$A_{ion} \propto \psi\left\{\frac{1 - e^{-2(A_0 + A_p)}}{2}\right\}\eta \tag{19}$$

where $\eta = A_0/(A_0 + A_p)$ is the fraction of perylene absorbance in the total absorption of a film sample, and A_p is the absorbance due to the polymer itself.

The perylene cation radical was produced with different yields in the polymers used. The highest yield of the perylene cation (i.e., the highest charge separation efficiency) was observed in PVBC, whereas the lowest yield was measured in PS, and intermediate yields were found in PC, PMMA, and PBM (Figure 5). This variation can be understood from the reactivity of polymers with the excess electrons. The quantum yield of charge separation ψ is determined by the competition between the geminate electron−cation recombination and the electron scavenging by polymer matrixes.

Polystyrene. A low yield of the perylene cation $\psi_{PS} = 2.4\%$ was observed in PS because PS does not react with excess electrons. The same is true of its model compounds benzene and toluene. Previous work on liquid benzene and toluene[32] found that electron attachment to the benzene ring is not favored unless very high pressures are used. The high pressure forces the localization of excess electrons by formimg the benzene and toluene anions. Under normal conditions, excess electrons

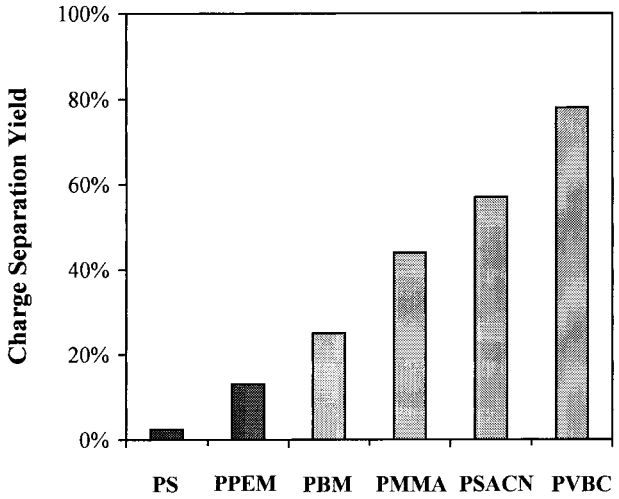

Figure 5. Charge separation yields in different polymers. Nitrogen laser was used as the excitation source.

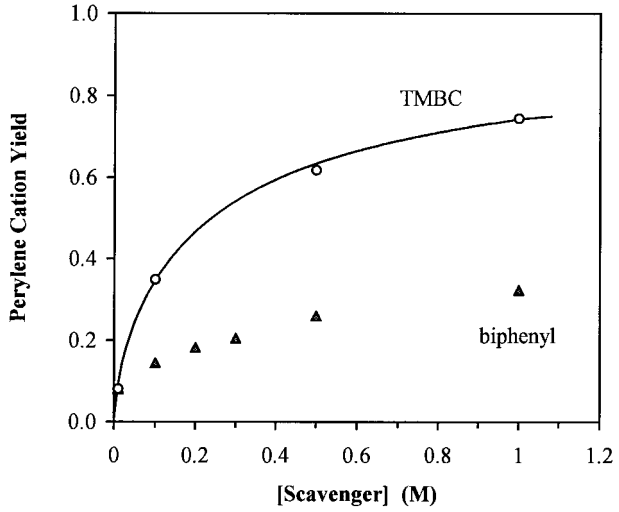

Figure 6. Increasing production of perylene cation radicals in polystyrene in the presence of electron scavengers sush as 2,4,6-trimethylbenzyl chloride (TMBC; circles) and biphenyl (triangles). ([TMBC] = 0, 0.1, 0.5, and 1 M; [Biphenyl] = 0, 0.1, 0.2, 0.3, 0.5, and 1 M.) The solid line shows the fitting using a diffsuion-controlled geminate ion recombination model in which electron distribution is described by a Gaussian function with $b_G = 32$ Å.

are only trapped to a very shallow depth in benzene and toluene and exhibit diffusivities on the order of 10^{-3} cm^2/s.[32] The same situation is expected for excess electrons in PS. High-energy radiation experiments have shown that the mobility of the quasi-free electrons in PS is on the order of 3×10^{-4} cm^2/s.[17] Geminate recombination between the perylene cation and the shallowly trapped excess electron occurs rapidly within ~1 ns. The low ion yield observed in PS is due to the fact that only a very small fraction of charge carriers escape the early recombination as free ions. Electron scavenging experiments were performed to help separate the geminate ion pairs. Different amounts of TMBC were doped into PS with perylene, and cation absorption at 545 nm was measured at 20 ns after the pulse. The increasing yields of the perylene cation with increasing TMBC concentration were simulated by the diffusion-controlled geminate recombination model (Figure 6). The parameter for the initial Gaussian distribution function $b_G = 32$ Å was obtained by fitting the scavenging pattern to eq 11. The electrons are ejected 36 Å on average away from the geminate perylene cation radicals in two-photon ionization at 337 nm, which compares well with the results of photoionization in liquid hydrocar-

bons.[13,14] The ion yield in a 5 mM perylene/PS film is predicted to be ~2.2% from the aforementioned simulation, in agreement with 2.4% measured relative to the ion yield $\psi_{PVBC} = 1$ in PVBC films. Addition of biphenyl also leads to enhanced production of the perylene cation. It is not surprising to notice that biphenyl exhibits a less efficient electron scavenging than TMBC, simply because of its lower reactivity with excess electrons.

Electron-scavenging components can be introduced in the PS matrix by copolymerization. A random copolymer of styrene and acrylonitrile was also examined in our studies. As shown earlier, perylene cations are easily produced in PSACN on excitation by 355-nm photons. For excitation at 337 nm, the charge separation yield of perylene is measured to be $\psi_{PSACN} = 0.57$ in PSACN, with 25% of acrylonitrile content (i.e., ~4.7 M). In both photochemistry and radiation chemistry, acetonitrile has been known to react with excess electrons and form an anion radical ($CH_3CN^{-\bullet}$).[33,34] The same reaction is responsible for the charge generation in PSACN:

$$e^- + >CHC{\equiv}N \rightarrow >CHC{\equiv}N^- \qquad (20)$$

Perylene cations are also produced in a 5 mM perylene-doped PACN film.

Polymethacrylates. The yields of charge separation in polyesters are $\psi_{PMMA} = 0.45$ for PMMA, $\psi_{PBM} = 0.25$ for PBM, and $\psi_{PPEM} = 0.13$ for PPEM. The ester group in the monomeric units of PMMA, PBM, and PPEM is at very high concentrations (6−8 M) in the solid polymers. The reaction of the ester group with excess electrons[35] leads to the formation of polymer anions and efficient charge separation. This result is confirmed by our transient absorption and dc-conductivity studies of photoionization in liquid acetate compounds (data not shown here). Electrons trapped in PMMA matrix have been studied by EPR spectroscopy by Tabata and Yamamoto.[36,37] A strong singlet peak was observed at the center of the EPR spectrum of irradiated PMMA at 77 K, which was assigned to an ester radical anion of PMMA ($PMMA^{-\bullet}$):

$$e^- + PMMA \rightarrow PMMA^{-\bullet} \qquad (21)$$

At 77 K, the $PMMA^{-\bullet}$ anion is not stable, and thermal fragmentation results in side chain scission and eventually leads to the formation of $P{-}COO^-$ and methyl radicals $\cdot CH_3$. At room temperature, the decarboxylation of $P{-}COO^-$ leads to the formation of the $CO_2^{-\bullet}$ anion radical and a main chain radical (P·), which further induces main chain scission:[36]

$$PMMA^{-\bullet} \rightarrow P - COO^- + \cdot CH_3 \rightarrow P\cdot + \cdot CO_2^- + \cdot CH_3 \qquad (22)$$

Similar processes occur in PBM and PPEM after electron trapping by the ester groups. Because the reactivity of these polymers with electrons is lower than that of PVBC, more electrons recombine with the parent cations before being trapped by the polymers. The higher yield of charge generation observed in PMMA than in PBM and PPEM might be attributed to the higher concentration of ester groups.

Poly(vinylbenzyl chloride). PVBC has a high concentration of chlorine atoms (7 M) that capture excess electrons efficiently via an electron-detachment reaction. This concentration corresponds to the high concentration limit of the electron scavenging in PS by TMBC. Electrons trapped in PVBC matrix exist as chloride anion Cl^-:

$$e^- + >CHC_6H_4CH_2Cl \rightarrow >CHC_6H_4CH_2^{\bullet} + Cl^- \qquad (23)$$

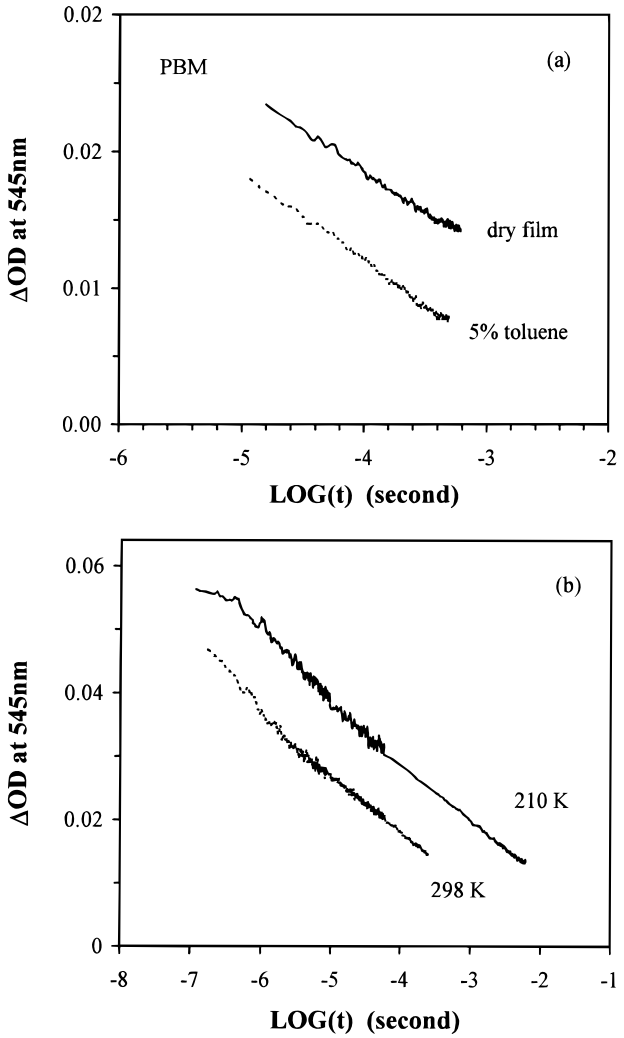

Figure 7. (a) Plasticization effect on perylene cation decay kinetics in a 5 mM Pe/PBM film ($\lambda_{ex} = 337$ nm). Key: (dashed line) wet film (~5% toluene); (solid line) dry film. (b) Temperature effect on charge recombination in PVBC as shown by a cooling-induced shift of decay trace on the semilog plot, from 298 K (dashed line) to 210 K (solid line).

Nearly 100% charge separation in PVBC ($\psi_{PVBC} = 1$) was confirmed by the electron-scavenging experiments in PS doped with TMBC to concentrations up to 1.0 M.

Charge Recombination: Mechanism and Kinetics. Recent work by Yamamoto and co-workers[38] indicated that thermalized electrons produced by photoionization of aromatic solutes are trapped in a bulk polymerized PMMA matrix. Long-range electron tunneling from the trapping sites back to the parent cations was suggested to explain the very slow decay (hours) of the ion radicals. Temperature also affected the recombination rate, and was attributed to the chain relaxation effect on the electron tunneling reaction in the PMMA matrix. In the present work, the effects of rigidity and temperature were examined to determine whether the recombination is diffusion controlled or it occurs via long-distance electron tunneling. A dry Pe/PBM film was compared with a slightly wet Pe/PBM film with ~5% toluene residue left in the film. A faster cation decay was observed in the wet film than in the dry PBM film. The perylene cations produced in these two films show parallel decay traces that are shifted along the log *t* axis relative to each other by approximately one unit (Figure 7a). This result is characteristic of the diffusion-controlled geminate ion recombination kinetics, indicating that all the elements involved in the ion

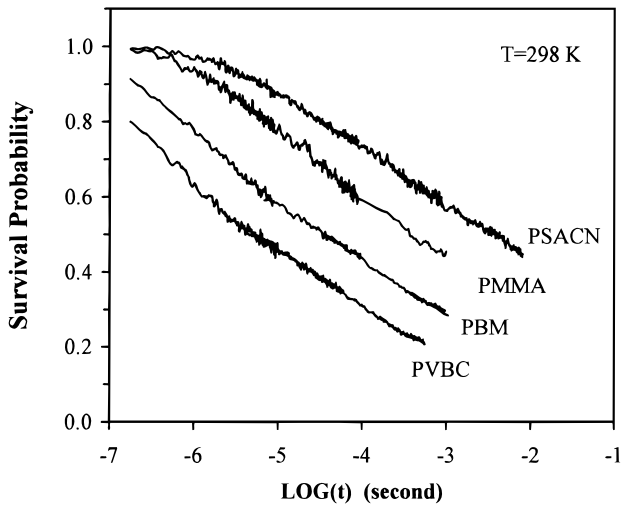

Figure 8. Decay kinetics of the perylene radical cations over a wide dynamic range in different polymers as indicated. Transient absorbance data are scaled to give relative yield (i.e., survival probability).

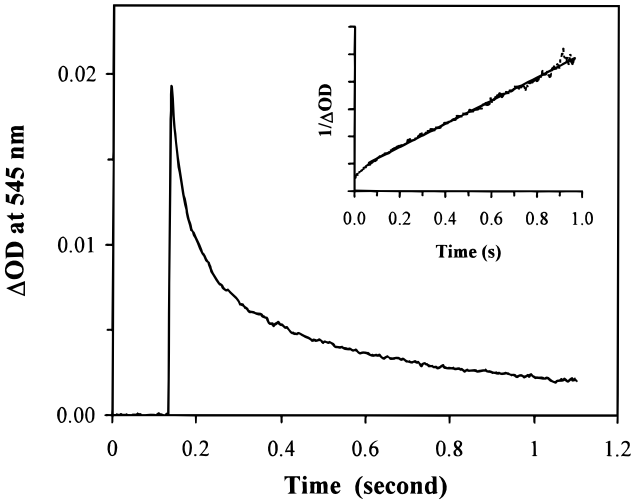

Figure 9. Charge recombination kinetics in a 5 mM Pe/PVBC film at the long time limit. Inset shows that the decay signal is fitted to a second-order recombination reaction after 0.1 s.

recombination process remain the same, apart from the diffusivity of the ionic species. The 10 times faster diffusion observed in the wet film compared with that in the dry one is solely due to the plasticization of PBM by the small amount of toluene. Similar plasticization effects on charge recombination has also been found in PVBC films.

Measurements on the cation decay kinetics were also made at low temperatures. Figure 7b shows two semilog decay traces of $Pe^{+\bullet}$ in a PVBC film at room temperature and 210 K. Lowering the sample temperature by 88 °C results in a significantly slower decay, which is shifted in parallel relative to the room-temperature curve by 1.2 units of log *t*. Again, only the diffusivity of ions (Cl^- for PVBC) is affected by the temperature because of the activated nature of molecular diffusion in a rigid polymer matrix ($T_g = 100-120$ °C). The activation energy for Cl^- anion diffusion in PVBC below the glass transition temperature is estimated to be ~16.4 kJ/mol. This value is somehow lower than the typical diffusion barrier ($E_a \approx 35$ kJ/mol) for small molecules such as O_2 and N_2 in glassy PS.[39]

The ion decay kinetics over a wide range of time was made in different polymers. Figure 8 shows the semilog plots of the perylene cation radical decay measured at room temperature in PVBC, PBM, PMMA, and PSACN with the time variation over seven orders of magnitude. On a short time scale ($10^{-8}-10^{-6}$ s) when there is no extensive molecular movement and charge carriers are relatively frozen, the cation radical decay cannot be well described by the diffusion model. Trapped charges at short separation might recombine via electron tunneling.[17] In this work, no such long-range recombination is observed for the anion fragments just mentioned.

In the middle range of the observation time window ($10^{-6}-10^{-3}$ s), a linear portion of the semilog plot exists for all the polymers studied. This result is characteristic of the diffusion-controlled geminate ion recombination kinetics,[40] as indicated by the simulation results:

$$\frac{C(t)}{C_0} = \text{constant} - k \log t \tag{24}$$

The slope *k* is a function of the Onsager length R_c and the distribution parameter b_G. Similar slopes were observed for PMMA and PBM films, indicating very close b_G (~32 Å) and R_c (within a range of 150−180 Å) values. The $Pe^{+\bullet}$ decay traces in PVBC, PBM, and PMMA were found to lie parallel to each other. The relative shift of these semilog curves along the log *t* axis is related to the variation in the diffusion constants *D* of the charge carriers in different polymers. The plot shows that Cl^- in PVBC moves six times faster than $CO_2^{-\bullet}$ in PBM, and about 60 times faster than $CO_2^{-\bullet}$ in PMMA. However, simulation of diffusion-controlled geminate ion recombination in this work and also in previous work by Noolandi[12] shows that the linear relation as given in eq 24 only lasts for two orders of magnitude in time for the typical b_G (~32 Å) and R_c (150−180 Å) values in the polymer systems already mentioned. The data in Figure 8 cannot be simply fitted to the model given in the simulation section. Such a prolonged charge recombination might be due to the nonhomogeneity of sites where ions are trapped to various depths. Instead of a single uniform diffusion constant characteristic of homogeneous media, a distribution of molecular diffusivities should be considered for amorphous polymeric solids. Nonexponential triplet quenching kinetics observed in amorphous polymers also indicates that molecular diffusion is dispersive in disordered solid systems.[31,41]

The long time decay above 100 ms can be fitted to a second-order homogeneous ion recombination because a small fraction of the ion pairs finally escape the geminate recombination and become free ions. These free ions uniformly spread over the polymer matrixes, and the recombination kinetics switches from geminate in nature to a homogeneous regime. Figure 7b shows that the free ion yield in PVBC is <7%. Because the cation has the same concentration as the trapped electron, the A + B type charge neutralization reaction shows the same second-order kinetics as an A + A type reaction:

$$\frac{1}{C(t)} = \frac{1}{C_0} + kt \tag{25}$$

For PVBC, a straight line is obtained on the 1/OD−t plot after ~100 ms (Figure 9), whereas for PMMA, a straight line is reached after ~1 s. The diffusion constants of the charge carriers were estimated from second-order rate constants to be 7.5×10^{-10} cm²/s in PVBC, 7.0×10^{-12} cm²/s in PMMA, and 2.2×10^{-10} cm²/s in PBM.[31] Because the large perylene cation moves about two orders of magnitude slower in glassy polymers, as shown by the triplet quenching studies,[31] the measured mobilities of the charge carriers are mainly due to Cl^- in PVBC,

and $CO_2^{-\bullet}$ in PBM and PMMA. The latter result confirms the chain scission reactions in PMMA and PBM after electron trapping. If we consider that these small ionic fragments move through many different sites in the homogeneous recombination, the diffusion rates just mentioned should be taken as values averaged over the ensemble of various sites in the disordered polymers.

The cation decay trace in PSACN, however, exhibits a much longer half-life of ~3 ms and does not lie parallel to those observed in PVBC, PBM, and PMMA (Figure 8). This trace cannot be understood by the same diffusion model used for the other three polymers, although they have fairly close b_G and R_c values, because of a fundamental difference in electron-trapping mechanisms. Electron trapping in PVBC, PBM, and PMMA occurs via a dissociative attachment that results in the small ionic fragments such as Cl^- and $CO_2^{-\bullet}$. In contrast, the electron attached to the cyano group (−C≡N) in PSACN is part of the polymer structure, and its translational movement is negligible in the glassy polymer on the experimental time scales. The activation energy measured from the temperature effect is ~7.3 kJ/mol (0.076 eV), which is significantly lower than that of Cl^- diffusion in PVBC. The distinct decay pattern and the low activation barrier indicate that the charge transport is not due to the diffusion of $Pe^{+\bullet}$. Instead, charge hopping among the cyano groups is responsible for the ion recombination in PSACN. The low transport barrier is in agreement with the low electron binding energy and the high reactivity of $CH_3CN^{-\bullet}$.[33]

Summary

Two different modes of photoinduced charge generation in polymers are examined in this work. Lower charge generation yield and shorter charge separation are generally observed in CT excitation than those in two-photon ionization. Such an excitation energy dependence of charge generation is further evident from the even larger charge separation distance (b_G = 54 Å) and the efficient ion production in electron-beam-irradiated PS.[17] Spectroscopic analysis of charge recombination kinetics suggests that two different modes of charge transport exist in solid polymers; namely, electronic hopping and molecular diffusion. Both modes are observed in low-energy photochemistry and high-energy radiation chemistry. Charge migration among the polymer-bound phenyl chromophores leads to the formation and subsequent recombination of matrix-separated ion pairs in TCNB-doped PS. Similar charge hopping among the cyano groups is responsible for the neutralization of $Pe^{+\bullet}$ in PACN. In the case of dissociative electron trapping in PVBC and polymethacrylates, charge recombination occurs via diffusion of small ionic fragments. The rigidity of the polymer matrixes does help to stabilize the charge carriers up to many microseconds for those generated in CT excitation and many milliseconds for those created in two-photon ionization. The ionic species trapped in solid polymers even live up to seconds in high-energy radiolysis experiments.[17]

Appendix

Scheme 2 illustrates the propagation of a laser pulse along the x-axis through a transparent films sample of thickness d. The film placed between $x = 0$ and $x = d$ contains a solute of concentration C_0, which absorbs at the wavelength of laser excitation with an extinction coefficient ϵ_0 and an absorbance $A_0 = C_0\epsilon_0 d$. These quantities are defined here for the natural logarithm notation used in the following equations, and they have a factor of 10 difference with regard to the conventional 10-based logarithm definition.

SCHEME 2: Propagation of a Laser Pulse through a Film Sample with a Thickness of *d* in Two-Photon Ionization Experiments

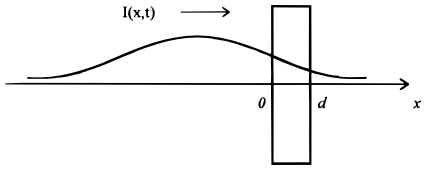

The propagation of the laser pulse through the sample is defined as a function of space x and time t using a Gaussian function:

$$I(x,t) = I_0(x,t)\,\pi^{-1/2}\exp\left\{-\left[\frac{t-(x/v-t_0)}{\delta t}\right]^2\right\} \text{ for } 0 \le x \le d \tag{A1}$$

where δt is the pulse width, which is ~5 ns in our experiments, and t_0 is the time the excitation pulse takes to travel from the laser to the sample. The pre-exponential factor $I_0(x,t)$, the intensity of the laser in number of photons per unit area per second, is a constant before entering the sample (i.e., $I_0(x,t) = I_0$) and generally a function of x and t inside the sample. The following coupled partial differential equations can be written for the laser pulse $I(x,t)$ inside the sample; that is, $0 \le x \le d$:

$$-\frac{\partial I(x,t)}{\partial x} = I(x,t)\,[C_0\epsilon_0 + C_1(x,t)\,\epsilon_1] \tag{A2}$$

$$\frac{\partial C_1(x,t)}{\partial t} = I(x,t)\,C_0\,\epsilon_0/N \tag{A3}$$

Here, $C_1(x,t)$ is the concentration of the solute S_1 state, ϵ_1 is its extinction coefficient at the same excitation wavelength, and N is the Avogadro number. If we notice $d/v \approx 10^{-12}$ s $\ll \delta t$, the exponential term in equation (A1) is a weak function of x and thus can be dropped out of the differentiation:

$$-\frac{\partial I_0(x,t)}{\partial x} = I_0(x,t)[C_0\,\epsilon_0 + C_1(x,t)\,\epsilon_1] \tag{A4}$$

Absorption of the second photon by the solute S_1 state leads to the formation of the Rydberg state from which ionization occurs with a quantum efficiency φ_{ion}. The concentration of the produced solute cation radicals $C_2(x,t)$ is defined by equation (A5):

$$\frac{\partial C_2(x,t)}{\partial t} = \varphi_{ion}\,I(x,t)\,C_1(x,t)\,\epsilon_1/N \tag{A5}$$

Assume that a fraction (ψ) of initially generated ion pairs escape the very fast electron−cation geminate recombination, leading to the charge separation measured on the nanosecond time scale. The end-of-pulse transient absorption of solute cation radicals with an extinction coefficient ϵ_2 at the monitoring wavelength (for example, λ = 545 nm for $Pe^{+\bullet}$) is given by the Lambert-Beer's law:

$$A_{ion} = \lim_{t\to\infty}\int_0^d \psi\,C_2(x,t)\,\epsilon_2\,dx \tag{A6}$$

The laser intensity inside the sample $I_0(x,t)$ can be solved from equations (A3) and (A4).

$$I_0(x,t) = \frac{I_0 \exp(-C_0 \epsilon_0 x)}{1 + \frac{\epsilon_1 I_0 \delta t}{N} erf\left(\frac{t - t_0}{\delta t}\right) \{1 - \exp(-C_0 \epsilon_0 x)\}} \quad \text{(A7)}$$

where $erf(x) = \pi^{-1/2} \int_{-\infty}^{x} \exp\{-\tau^2\}\, d\tau$ is the error function.

For the excitation conditions used in our experiments, $\epsilon_1 I_0 \delta t/N \approx 10^{-2} \ll 1$, and $I_0(x,t)$ can be simply written as follows:

$$I_0(x,t) = I_0 \exp(-C_0 \epsilon_0 x) \quad \text{(A8)}$$

Integration of equation (A6) gives the cation radical absorption, which was measured ~20 ns after the laser pulse in the experiments.

$$A_{ion} = \psi \varphi_{ion} \left(\frac{I_0 \delta t}{N}\right)^2 \epsilon_1 \epsilon_2 \lim_{t \to \infty} \Phi\left(\frac{t - t_0}{\delta t}\right) \times \left\{\frac{1 - \exp(-2C_0 \epsilon_0 d)}{2}\right\} \quad \text{(A9)}$$

where $\Phi(x)$ is a self overlap integral of the laser pulse:

$$\Phi(x) = \pi^{-1/2} \int_{-\infty}^{x} erf(\tau) \exp\{-\tau^2\}\, d\tau \quad \text{(A10)}$$

Therefore, measurements of perylene absorbance at the excitation wavelength (A_0) and end-of-pulse transient absorption of $Pe^{+\bullet}$ (A_{ion}) in a polymer film could be quantitatively related to the charge separation yield ψ:

$$A_{ion} \propto \psi \left(\frac{1 - e^{-2A_0}}{2}\right) \quad \text{(A11)}$$

Acknowledgment. The authors thank the National Science Foundation for financial support of this work.

References and Notes

(1) Mort, J.; Pfister, G. In *Electronic Properties of Polymers*; Mort, J., Pfister, G., Eds.; John Wiley & Sons: New York, 1982; Chapter 6 and references therein. (b) Pai, D. M. In *Photoconductivitty in Polymers: An Interdisciplinary Approach*; Patsis, A. V., Seanor, D. A., Eds.; Technomic: Westport, CT, 1976; Chapter 2.

(2) Law, K.-Y. *Chem. Rev.* **1993**, *93*, 449 and references therein.

(3) Haarer, D. *Angew. Makromol. Chem.* **1990**, *183*, 197.

(4) Onsager, L. *Phys. Rev.* **1938**, *54*, 554.

(5) Melz, P. J. *J. Chem. Phys.* **1972**, *57*, 1694.

(6) Danelyus, R.; Rotomski, R. *Sov. J. Quantum Electron.* **1982**, *12*, 994.

(7) Walsh, C. A.; Burland, D. M. *Chem. Phys. Lett.* **1992**, *195*, 309.

(8) Miyasaka, H.; Moriyama, T.; Kotani, S.; Muneyasu, R.; Itaya, A. *Chem. Phys. Lett.* **1994**, *225*, 315.

(9) Ueda, T.; Fujisawa, R.; Fukumura, H.; Itaya, A.; Masuhara, H. *J. Phys. Chem.* **1995**, *99*, 3630. (b) Watanabe, K.; Asahi, T.; Masuhara, H. *Chem. Phys. Lett.* **1995**, *233*, 69. (c) Watanabe, K.; Asahi, T.; Masuhara, H. *J. Phys. Chem.* **1996**, *100*, 18436.

(10) Yokoyama, M.; Endo, Y.; Matsubara, A.; Mikawa, H. *J. Chem. Phys.* **1981**, *75*, 3006.

(11) Braun, C. L. *J. Chem. Phys.* **1984**, *80*, 4157.

(12) Noolandi, J.; Hong, K. M. *J. Chem. Phys.* **1978**, *68*, 5163. (b) Hong, K. M.; Noolandi, J. *J. Chem. Phys.* **1979**, *70*, 3230. (c) Noolandi, J. In *Kinetics of Nonhomogeneous Processes*; Freeman, G. R., Ed.; John Wiley & Sons: New York, 1987; Chapter 9, p 465.

(13) Thomas, J. K.; Piciulo, P. L. *J. Chem. Phys.* **1978**, *68*, 3260.

(14) Scott, T. W.; Braun, C. L. *Chem. Phys. Lett.* **1986**, *127*, 501.

(15) Freeman, G. R. In *Kinetics of Nonhomogeneous Processes*; Freeman, G. R., Ed.; John Wiley & Sons: New York, 1987; Chapter 2, p 19.

(16) Beck, G.; Thomas, J. K. *J. Phys. Chem.* **1972**, *76*, 3856.

(17) Zhang, G.; Thomas, J. K. *J. Phys. Chem.* **1996**, *100*, 11438.

(18) Tachiya, M.; Mozumder, A. *Chem. Phys. Lett.* **1975**, *34*, 77.

(19) Hummel, A.; Infelta, P. P. *Chem. Phys. Lett.* **1974**, *24*, 559.

(20) Smith, G. D. *Numerical Solution of Partial Differential Equations: Finite Difference Methods*, 3rd ed.; Clarendon: Oxford, 1985.

(21) Ojima, S.; Miyasaka, H.; Mataga, N. *J. Phys. Chem.* **1990**, *94*, 4147.

(22) Tsujii, Y.; Takami, K.; Tsuchida, A.; Ito, S.; Yamamoto, M. *Macromolecules* **1993**, *26*, 1411. (b) Masuhara, H.; Vandendriessche, J.; Demeyer, K.; Boens, N.; De Schryver, F. C. *Macromolecules* **1982**, *15*, 1471. (c) Sakai, H.; Itaya, A.; Masuhara, H. *J. Phys. Chem.* **1989**, *93*, 5351. (d) Masuhara, H.; Itaya, A. In *Dynamics and Mechanisms of Photoinduced Electron Transfer and Related Phenomena*; Mataga, N., Okada, T., Masuhara, H., Eds.; Elsevier: Amsterdam, 1992; p 363.

(23) Tsuchida, A.; Yamamoto, M.; Nishijima, Y. *J. Phys. Chem.* **1984**, *88*, 5062.

(24) Lamola, A.; Hammond, G. *J. Chem. Phys.* **1965**, *43*, 2129. (b) Carmichael, I.; Hug, G. L. *J. Phys. Chem. Ref. Data* **1986**, *15*, 1.

(25) Gould, I. R.; Noukakis, D.; Gomez-Jahn, L.; Goodman, J.; Farid, S. *J. Am. Chem. Soc.* **1993**, *115*, 4405. (b) Asahi, T.; Ohkohchi, M.; Mataga, N. *J. Phys. Chem.* **1993**, *97*, 13132.

(26) Muller-Horsche, E.; Haarer, D.; Scher, H. *Phys. Rev. B* **1987**, *35*, 1273.

(27) Zhang, G.; Thomas, J. K. *J. Phys. Chem.* **1995**, *99*, 11203.

(28) Hirsch, J. *J. Phys. C* **1979**, *12*, 321. (b) Reimer, B.; Bassler, H. *Phys. Stat. Sol. A* **1979**, *51*, 445.

(29) Tsujii, Y.; Tsuchida, A.; Yamamoto, M.; Nishjima, Y. *Macromolecules* **1988**, *21*, 665. (b) Tsujii, Y.; Tsuchida, A.; Onogi, Y.; Yamamoto, M. *Macromolecules* **1990**, *23*, 4019.

(30) Giro, G.; Di Marco, P. G. *Chem. Phys. Lett.* **1989**, *162*, 221.

(31) Zhang, G.; Thomas, J. K. In *Irradiation of Polymers: Fundamentals and Technological Applications*; Shalaby, S. W., Clough, R. L., Eds.; *ACS Symp. Ser.*, Vol. 620, 1996; Chapter 4.

(32) Itoh, K.; Holroyd, R. *J. Phys. Chem.* **1990**, *94*, 8850; *J. Phys. Chem.* **1990**, *94*, 8854.

(33) Bell, I. P.; Rodgers, M. A. J. *J. Chem. Soc., Faraday Trans. 2* **1977**, *73*, 315.

(34) Hirata, Y.; Mataga, N.; Sakata, Y.; Misumi, S. *J. Phys. Chem.* **1982**, *86*, 1508. (b) Hirata, Y.; Takimoto, M.; Mataga, N. *Chem. Phys. Lett.* **1983**, *97*, 569.

(35) Tachikawa, H.; Yoshida, H.; Ogasawara, M. *Radiat. Phys. Chem.* **1991**, *37*, 107 and references therein.

(36) Tabata, M.; Nilsson, G.; Lund, A. *J. Polym. Sci., Polym. Chem. Ed.* **1983**, *21*, 3257.

(37) Sakai, W.; Tsuchida, A.; Yamamoto, M.; Matsuyama, T.; Yamaoda, H. *Makromol. Chem., Rapid Commun.* **1994**, *15*, 551.

(38) Tsuchida, A.; Sakai, W.; Nakano, M.; Yoshida, M.; Yamamoto, M. *Chem. Phys. Lett.* **1992**, *188*, 254.

(39) Krevelen, V. *Properties of Polymers*, 3rd ed.; Elsevier Science: Amsterdam, 1990; p 544.

(40) Debye, P.; Edwards, J. O. *J. Chem. Phys.* **1952**, *20*, 236.

(41) Masoumi, Z.; Stoeva, V.; Yekta, A.; Pang, Z.; Manners, I.; Winnik, M. A. *Chem. Phys. Lett.* **1996**, *261*, 551.